



Development of stable and efficient CeVO₄ systems for the selective reduction of NO_x by ammonia: Structure-activity relationship

Sylvain Gillot^a, Grégory Tricot^b, Hervé Vezin^b, Jean-Philippe Dacquin^a, Christophe Dujardin^a, Pascal Granger^{a,*}

^a Unité de Catalyse et de Chimie du Solide, UMR8181, Université de Lille Sciences et Technologies, Ecole Nationale Supérieure de Chimie de Lille, Bâtiment C3, 59650 – Villeneuve d'Ascq, France

^b Laboratoire de Spectrochimie Infrarouge et Raman, UMR CNRS 8516, Bâtiment C5 – UMR CNRS 8516, 59650 – Villeneuve d'Ascq, France

ARTICLE INFO

Article history:

Received 6 February 2017

Received in revised form 24 May 2017

Accepted 17 June 2017

Available online 23 June 2017

Keywords:

Ammonia

CeVO₄

Fast-SCR

Selective catalytic reduction

NO_x

ABSTRACT

Bulk CeVO₄ catalysts prepared by hydrothermal synthesis have been developed for the ammonia-selective catalytic reduction of NO_x to nitrogen. The catalytic properties were evaluated in standard- and fast-SCR conditions for stationary and mobile applications. The coexistence of low concentration of Ce⁴⁺ species stabilized as CeO₂ with bulk CeVO₄ was found to be crucial for enhancing the intermediate formation of NO₂ from NO oxidation. Such cooperative effects impact on the rate of NO conversion to nitrogen regardless of the operating conditions. Aging processes under wet atmosphere at 500 °C and 600 °C did not destabilize the bulk zircon-type structure of CeVO₄. No loss of vanadium was observed due to significant sublimation of vanadium. Despite poorer textural properties with regard to fresh CeVO₄, aged CeVO₄ catalysts exhibit better catalytic properties in terms of rate of NO conversion and selectivity thus providing an alternative to less stable supported vanadia-based catalysts. Indeed, higher TOF values were measured in standard-SCR conditions at 200 °C on aged samples at 600 °C whereas an aging at 500 °C leads to selectivity enhancement at high temperature. All these changes can be rationalized based on the surface modifications of redox and acidic properties of vanadium species due to a slight extraction and stabilization of VO_x species.

© 2017 Elsevier B.V. All rights reserved.

1. Introduction

The Selective Catalytic Reduction of NO_x by ammonia is a widespread abatement technology to treat the atmospheric pollutant emissions from stationary sources [1–9]. Supported vanadium based catalysts are the current benchmark catalysts typically running in standard-conditions according to Eq. (1).



Numerous investigations were performed to establish relevant structural-reactivity relationships [8–10] and to elucidate the reaction mechanism. It was suggested that the SCR reaction occurs through a redox mechanisms involving gas-phase or weakly adsorbed NO species and ammonia bonded on Lewis acid sites [8,11,12] or on Brønsted acid sites [4,6]. Most of those investigations pointed out the complexity of the surface processes and a distribution of the reactivity depending on the vanadium coverage with the

existence of monomeric, dimeric, polymeric VO_x entities [9] and on the chemical environment at the vicinity of vanadate species [9]. Diverse explanations were suggested in order to explain the observed rate enhancements ascribed to an increase of the redox properties, the creation of new Brønsted acid sites, the requirement of a dual site mechanism. Basically, V⁵⁺–OH would serve as acid site for ammonia adsorption, then adsorbed ammonia would be activated on a redox V⁵⁺ = O site further reduced to V(+IV) species and reoxidized with gaseous oxygen.

SCR Technology is still a matter of interest for designing efficient processes for mobile sources to meet stringent standard regulations for Diesel engines [13–20]. In this last case, different, kinetic regimes can occur depending on the NO/NO_x ratio corresponding to standard- or preferentially the fast-SCR conditions according to reaction (2).



It has been shown that the reaction mechanism essentially differs from the reoxidation of V(+IV) species to V⁵⁺ = O occurring more readily in the presence of NO₂ than O₂ for the standard-SCR. In practice, the development of conventional V₂O₅/WO₃/TiO₂ catalysts for

* Corresponding author.

E-mail address: pascal.granger@univ-lille1.fr (P. Granger).

mobile applications is limited due to the weak resistance of well-dispersed VO_x species to thermal sintering [14]. Their aggregation can lead ultimately to formation of V_2O_5 nanoparticles which can sublime above 650 °C accompanied with a greater production of N_2O as potent greenhouse gas [21].

Ceria incorporation to vanadium based catalysts contributed to significant improvements in terms of activity ascribed to a higher resistance to deactivation phenomena in more realistic SCR conditions i.e. in the presence of water, CO_2 and propene [22]. Typically, different supported 2D- VO_x species are characterized by different thermal stabilities according to the nature of the support. Previous investigations pointed out the stronger interaction between vanadia and ceria compared to alumina and silica which allows a higher dispersion limit in between 9 and 12 V atoms per nm^2 of ceria support [23]. Numerous investigations demonstrated the beneficial effect of Ce incorporation to V_2O_5 - WO_3 / TiO_2 [24]. By way of illustration, Chen et al. [24] found a greater stabilization of Ce^{3+} in mixed oxide catalysts then enhancing the rate of NO oxidation to NO_2 and the acidic properties through the creation of more active Brønsted acid sites. Earlier investigations also underlined the high thermal stability of zircon-type CeVO_4 which forms in air above 750 °C from VO_x/CeO_2 [25]. Presently, the distribution of the reactivity on $\text{V}_2\text{O}_5/\text{CeO}_2$ mixed oxide is somewhat complex to understand properly because of the formation of CeVO_4 and subsequent correlation of V-O-Ce entities as active sites present on both systems VO_x/CeO_2 and $\text{CeVO}_4/\text{CeO}_2$.

The present study is devoted to the development of thermally stable bulk CeVO_4 catalysts for the selective reduction of NO_x by ammonia. Such an objective might represent a significant outcome compared to less stable benchmark supported vanadia-based catalysts. It will be also found that the coexistence of CeO_2 with CeVO_4 and the impact of thermal aging on the surface properties led to unexpected catalytic properties on aged catalysts compared to freshly-prepared CeVO_4 . The comparison between acidic and redox properties of fresh and aged samples provides original information which could be valuable for further optimization of CeVO_4 catalytic systems.

2. Experimental

2.1. Catalyst preparation

CeVO_4 was synthesized via a hydrothermal route as described elsewhere [26]. Na_3VO_4 (99.98% Sigma-Aldrich) was dissolved in 50 mL of dionized water under vigorous stirring. The pH value was adjusted to 1.8 by adding dropwise an aqueous solution of nitric acid (3 M). In those operating conditions VO_2^+ cations were likely stabilized in aqueous phase. In a second step, an aqueous solution was prepared after dissolution of the precursor salt $\text{Ce}(\text{NO}_3)_3 \cdot 6\text{H}_2\text{O}$ (99%, Sigma-Aldrich). This second solution was added to the former one containing VO_2^+ cations. Afterwards, a progressive addition dropwise of an aqueous solution of sodium hydroxide (1 M) until the stabilization of the pH value to 8.5 induced the precipitation of cerium and vanadium as hydroxide precursors. The suspension thus obtained was hydrothermally treated at 180 °C for 24 h leading to the formation of the CeVO_4 zircon-type structure. At the end of the hydrothermal treatment, a significant shift on the pH value from 8.5 to 3.3 occurred in accordance with earlier observations [27]. The CeVO_4 sample as-prepared was separated by centrifugation, then abundantly washed with dionized water and ethanol and finally dried in air at 80 °C for 24 h. This sample was labeled “fresh” CeVO_4 in the text of this manuscript. The fresh sample was further aged at 500 °C and 600 °C for 5 h in a gas mixture composed of 10 vol.% H_2O diluted in air with a residence time of 0.024 g h L⁻¹. The elemental compositions listed in Table 1 were measured by Energy

Table 1

Elemental analysis, textural and structural properties of CeVO_4 catalysts freshly-prepared from hydrothermal synthesis and after aging.

Catalyst	Elemental composition (%)		Specif. Surf. Area ($\text{m}^2 \text{g}^{-1}$)	Crystallite size d (nm)	
	Ce	V		CeVO_4	CeO_2
Fresh	50.7	49.3	46.6	27	46
After SCR reaction ^a	n.m.	n.m.	36.3	34	45
Aged at 500 °C	49.2	50.8	17.7	46	46
Aged at 600 °C	50.1	49.9	5.8	85	57

^a After exposure to successive TPR reaction experiments with different molar NO/NO_x ratio.

Dispersive X-ray Spectroscopy. As seen, no loss of vanadium species occurred during aging.

2.2. Physicochemical characterization

2.2.1. Bulk characterization

X-Ray diffraction (XRD) analysis was performed at room temperature on a Bruker AXS D8 Advance diffractometer running in Bragg-Brentano geometry fitted with a LynxEye Super Speed detector. XRD data were collected with $\text{Cu K}\alpha$ radiation ($\lambda = 0.154 \text{ nm}$, 40 kV, 30 mA) in the 10–80° 2 θ range with a 0.02° 2 θ step.

Raman spectroscopic measurements were carried out on a Labram HR Jobin Yvon spectrometer by using an excitation wavelength of 532 nm. A 100 \times microscope objective was utilized for focusing the excitation beam and collecting the scattered light. A silicon line at 520 cm^{-1} was used for calibration prior to each measurement.

H_2 -Temperature-Programmed Reduction experiments (H_2 -TPR) were performed on a Micromeritics Autochem II 2920 instrument with a flow of 5 vol.% H_2 diluted in Ar and a constant heating rate of 10 °C/min.

The different CeVO_4 samples were analysed using ^{51}V magic angle spinning nuclear magnetic resonance (MAS-NMR) experiments performed at 210.4 MHz on a 18.8 T AVANCE III Bruker spectrometer equipped with a 3.2 mm probe head operating at a spinning frequency of 20 kHz. The spectra were recorded with a 0.5 μs pulse length (corresponding to a $\pi/12$ flip angle), 1024 transients and a recycle delay of 0.5 s. The ^{51}V chemical shifts were referred to VOCl_3 solution as 0 ppm.

Continuous wave electronic paramagnetic resonance (CW-EPR) experiments were performed at room temperature on an X-band ELEXYS E580 Bruker spectrometer. The spectra were acquired with 256 transients, 2 mW of microwave power and 2 G of modulation amplitude.

2.2.2. Surface characterization

XPS experiments were carried out on an AXIS Ultra DLD Kratos spectrometer equipped with a mono-chromatized aluminium source for excitation (150 W). Binding energies (B.E.) values were referenced to the O 1s core level at 530.5 eV.

Infrared spectroscopic measurements during pyridine adsorption-desorption experiments were carried out on a Nicolet Protégé 460 infrared spectrometer. Prior to pyridine adsorption at room temperature, samples were outgassed under vacuum (10^{-3} mbar) at 450 °C. IR spectra were recorded after evacuation at different temperatures in the range 25–250 °C. The values of the absorption coefficients used for the quantification of Lewis and Brønsted acid sites after integration of infrared bands were respectively 1.5 $\text{cm} \mu\text{mol}^{-1}$ and 1.8 $\text{cm} \mu\text{mol}^{-1}$ as reported elsewhere [28].

Specific surface area was measured by N_2 physisorption at -196 °C with a Flowsorb III device. Prior to nitrogen physisorption,

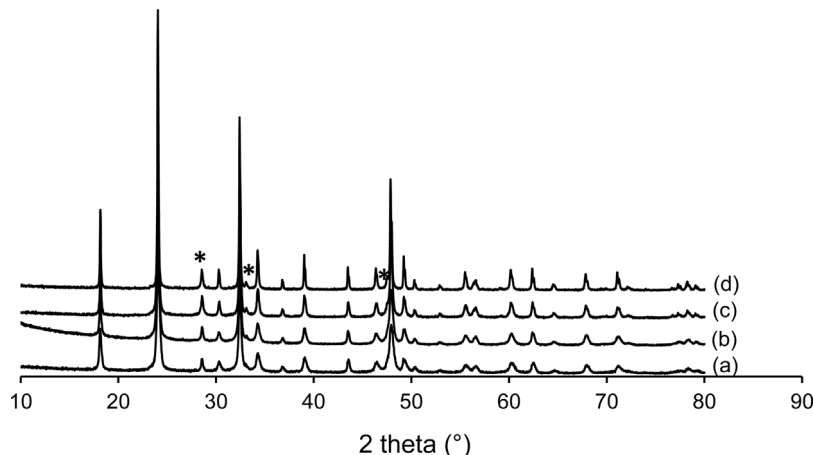


Fig. 1. XRD patterns characteristic of the zircon-type structure of CeVO_4 on fresh sample (a), after SCR reaction (b), aged in ex situ conditions in wet atmosphere (air + 10 vol.% H_2O) at 500°C (c), aged at 600°C (d) – (*) Characteristic reflections of the cubic structure of CeO_2 .

the samples were outgassed under vacuum at 100°C for 1 h under a flow of helium.

2.3. Catalytic measurements

Catalytic properties were evaluated from Temperature-Programmed Reaction (TPR) experiments by using 80 mg (W) of catalyst in powder form with grain size in the range 150–300 μm diluted in 1 g SiC in a plug flow reactor. A constant heating rate of $2^\circ\text{C}/\text{min}$ was maintained up to the final temperature. The total flow rate F_0 of 20 L h^{-1} corresponded to a time residence W/F_0 of $4 \times 10^{-3} \text{ g.h.L}^{-1}$. The composition of the reaction mixture was 400 ppm NH_3 , 400 ppm NO_x , 8 vol.% O_2 , 10 vol.% CO_2 , 10% H_2O diluted in He. Temperature-programmed conversion and selectivity curves were recorded for different molar NO to NO_x ratios of 0.5 and 1 corresponding to fast- and standard-SCR conditions respectively. The calculation of N_2 and N_2O concentrations was carried out from online Varian CP-4900 μGC analyses after separation of the reactants and products on two distinct columns (molecular sieve 5 Å and porapak Q). The concentration of NO_x , NO, NO_2 , NH_3 were determined from infrared analysis by using an IGS Antaris NO_x spectrometer supplied by Thermo Scientific.

Preliminary, kinetic experiments on fresh CeVO_4 in the temperature range 200 – 300°C did not reveal significant deviations in the rate of NO conversion by modifying the catalyst loading at constant space velocity suggesting that external diffusion should not occur significantly on the fresh CeVO_4 sample.

3. Results

3.1. Bulk physicochemical characterization of CeVO_4

3.1.1. X-ray diffraction analysis

XRD patterns recorded on powder samples are reported in Fig. 1. The most intense signals at $2\theta = 24.0^\circ$, 32.3° and 47.8° can be assigned to the characteristic (200), (112) and (312) reflections of the tetragonal structure of CeVO_4 (JCPDS 00-012-0757) on fresh and aged samples. Additional reflections appear notably the most intense at $2\theta = 28.5^\circ$ characterizing the cubic structure of CeO_2 (JCPDS 01-081-0792). As reported elsewhere, the formation of ceria could be explained by the dehydration of $\text{Ce}(\text{OH})_3$ during the hydrothermal synthesis and subsequent oxidation with air into CeO_2 [29]. Average crystallite size diameters have been estimated by using the Scherrer equation and considering the most intense reflections for CeVO_4 and CeO_2 . The comparison of the crystallite

size values at increasing aging temperature (see Table 1) underlines a greater sensitivity of CeVO_4 to thermal sintering compared to CeO_2 especially after aging at 600°C .

3.1.2. Raman spectroscopy

As illustrated in Fig. 2, different Raman bands characterize CeO_2 , V_2O_5 and composite mixed oxides CeVO_x . As seen, CeO_2 exhibits an intense and narrow band at 466 cm^{-1} previously ascribed to the F_{2g} vibration of the characteristic cubic fluorite structure of CeO_2 . The Raman bands observed on pure V_2O_5 at 994 cm^{-1} and below 800 cm^{-1} are characteristic of V_2O_5 , $\text{V}=\text{O}$ bond and $\text{V}=\text{O}-\text{V}$ structure corresponding to the stretching vibration mode of polyvanadate species [30,31].

Figs. 2(c)–(e) correspond to Raman spectra recorded on fresh CeVO_4 and then aged at 500°C and 600°C . The absence of Raman band in the region 800 – 1000 cm^{-1} characterizing V_2O_5 is remarkable emphasizing the structural stability of CeVO_4 . A sharp decrease in intensity of the 467 cm^{-1} Raman band corresponding to the stretching vibration of the $\text{Ce}=\text{O}$ bond in CeO_2 is also observable. New Raman bands appear at 261 , 383 , 788 , 800 and 863 cm^{-1} characterizing CeVO_4 in agreement with previous assignments [32,33]. The Raman band at 863 cm^{-1} confirms the tetrahedral environment of vanadium in the zircon-type structure of CeVO_4 . The Raman bands at 863 cm^{-1} can be ascribed to $\text{A}1\text{g}$ vanadate symmetric stretching (ν_1), E_g and B_{2g} antisymmetric stretching mode of vanadate (ν_3) correspond to the 800 and 788 cm^{-1} signals whereas Raman bands at 467 and 383 cm^{-1} can be associated to the B_{2g} and B_{1g} deformations (ν_4 and ν_2).

3.1.3. EPR and ^{51}V RMN spectroscopy

The ^{51}V NMR spectra obtained on the different CeVO_4 samples are displayed in Fig. 3. All the analyses present a main component (denoted as (1)) at -437 ppm accompanied by numerous spinning sidebands (denoted with *). While the chemical shift value is in a good agreement with previous studies of CeVO_4 [34,35], an unreported weak deshielding effect can be observed on the thermally treated samples, probably due to slight structural rearrangements. It is also noteworthy that no signal is observed at -609 ppm (corresponding to the V_2O_5 compound (Fig. 3e)), indicating that all the CeVO_4 samples can be considered free of any vanadium pentoxide traces, as previously shown by the XRD and Raman spectroscopy results.

EPR spectra collected in Fig. 4 did not reveal significant information in spite of very long acquisition time (8 h per analysis). Only broad and weak signals on the fresh CeVO_4 sample (signal (1)) which has not been assigned (see Fig. 4(a)). A broad signal appears

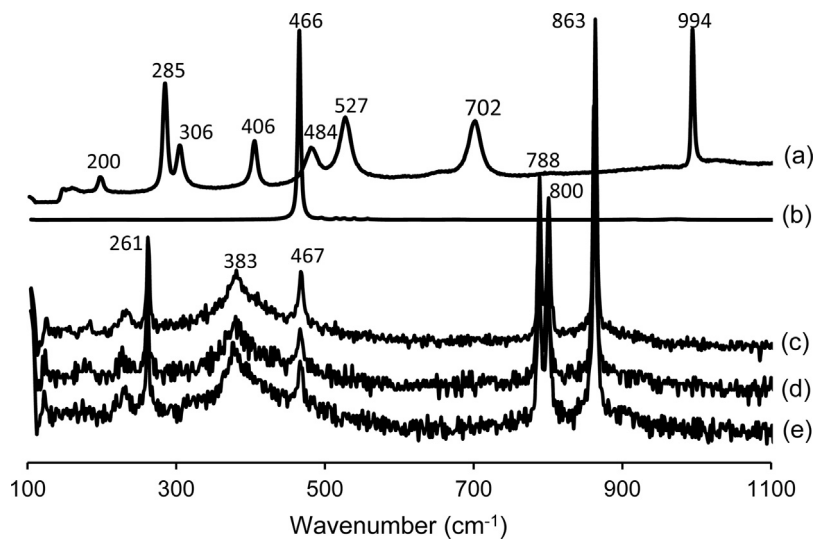


Fig. 2. Raman spectra recorded on V₂O₅ (a), CeO₂ (b) and CeVO₄ after aging in ex situ conditions in wet atmosphere (air + 10 vol.% H₂O) at 500 °C (c) and 600 °C (d), fresh CeVO₄ sample (e).

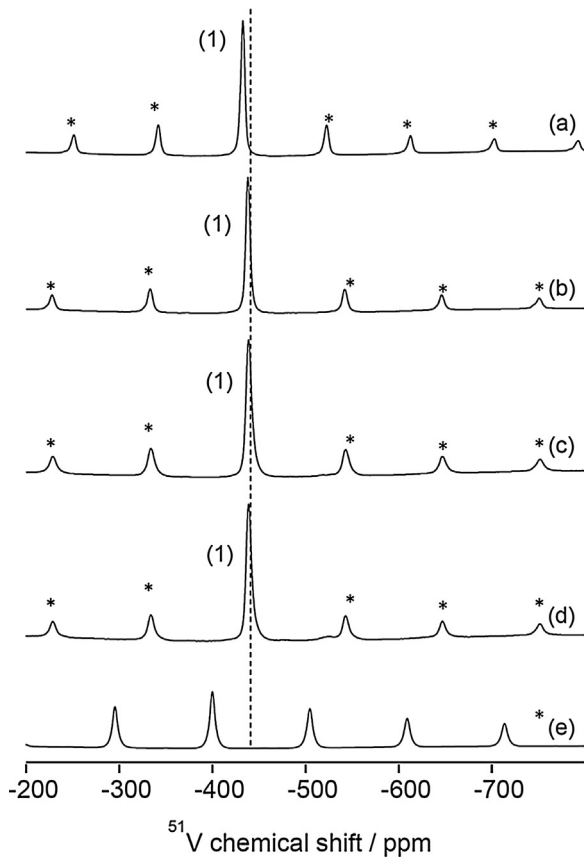


Fig. 3. ⁵¹V NMR spectra recorded on CeVO₄ aged at 600 °C (a); aged at 500 °C (b); used CeVO₄ after SCR reaction (c); Fresh CeVO₄ sample (d); reference V₂O₅ sample (e).

on used CeVO₄ after SCR reaction (signal (3) in Fig. 4(d)). This broad signal of 2000 G linewidth is typical of superparamagnetic signal as observed in iron oxide phases. This broad line resulting from a collective magnetism shows a ferromagnetic behaviour as indicated by the intensity increase and the displacement to the low region of this signal in the experiment performed at -268 °C. The Fig. 4(b) and Fig. 4(c) show that a weak ill-defined signal can be also observed on the spectra recorded on the 500 °C and 600 °C aged samples (sig-

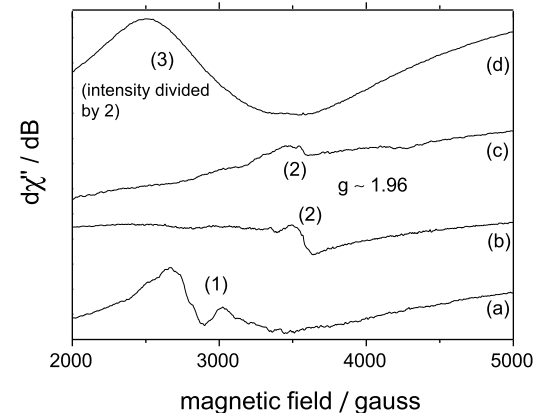


Fig. 4. EPR spectra recorded on fresh CeVO₄ (a); after aging at 500 °C (b); after aging at 600 °C (c) used CeVO₄ after SCR reaction (d). The intensity of the (d) spectrum has been divided by 2.

nal (2)). This signal centered at $g \sim 1.96$ indicates the presence of d^1 that can be ascribed to paramagnetic V⁴⁺ species. As ⁵¹V has a nuclear spin $I = 7/2$ then we can expect a hyperfine coupling of $S = 1/2$ with the nuclear spin which can provide hyperfine structure in the spectrum. In this study, we are more in the case of polaron system with a free electron that surrounding vanadium moieties but with no d-orbital localization. Similar observations were earlier reported on VO_x/Al₂O₃ calcined at 500 °C [36] and fumed vanadia samples [37]. Prakash and Kevan [38] as well as Conception et al. [36] also observed the development of hyperfine structures after subsequent reduction arising from the magnetic interaction of the unpaired electron with the ⁵¹V nucleus ascribed to isolated VO²⁺ cations in square pyramidal or distorted octahedral environment. Such hyper structure is not observed in Fig. 4. However, the presence of trace amount of V⁴⁺ species on aged CeVO₄ samples at 500 °C is in relative good agreement with previous observations on calcined V₂O₅–WO₃/Al₂O₃ showing a relative increase in V(+IV) species with a rise in calcination temperature up to 900 °C ascribed to the agglomeration of isolated vanadyl species into polymeric ones [39]. Interestingly, the signal at $g \sim 1.96$ persists on aged sample at 600 °C.

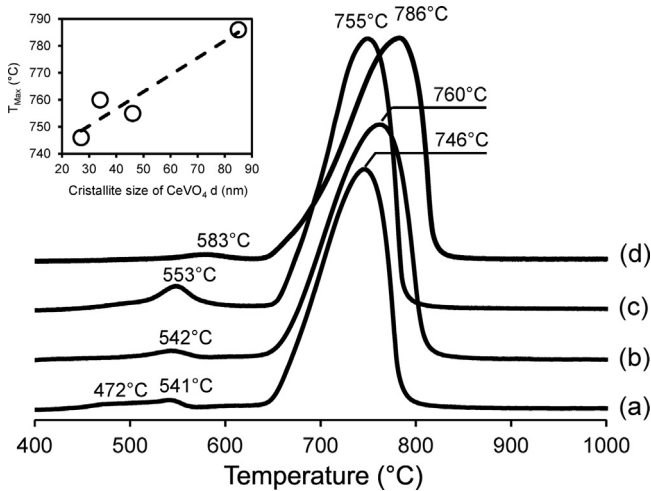


Fig. 5. H₂-Temperature-programmed consumption profile vs. temperature recorded on Fresh CeVO₄ (a); after SCR reaction (b); after aging in ex situ conditions in wet atmosphere (air + 10 vol.% H₂O) at 500 °C (c) and 600 °C (d).

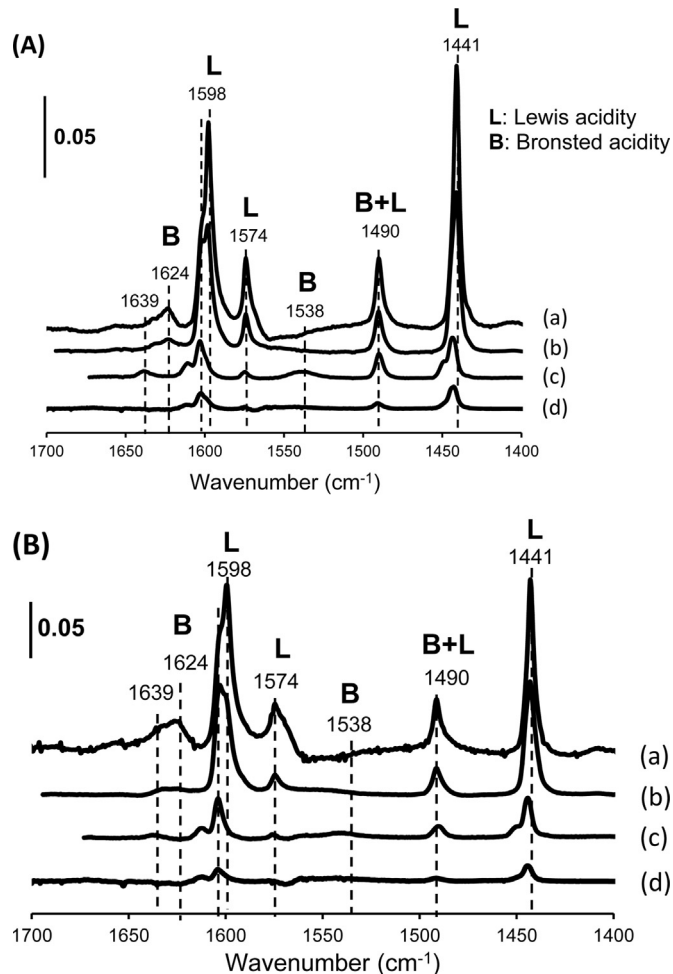


Fig. 6. FTIR spectra of adsorbed pyridine at 100 °C (A) and 150 °C (B) on fresh CeVO₄ (a); after SCR reaction (b); after aging in ex situ conditions in wet atmosphere (air + 10 vol.% H₂O) at 500 °C (c) and 600 °C (d) – Prior to pyridine adsorption at room temperature, samples were outgassed under vacuum (10⁻³ mbar) at 450 °C.

3.1.4. Reducibility of CeVO₄ samples

As shown in Fig. 5, H₂ consumption profiles vs. temperature are dominated by a prominent H₂-consumption signal in the range 640–850 °C ascribed to bulk reduction processes. Broad and weak contributions also appear below 590 °C more distinctly on CeVO₄ aged at 500 °C. These observations agree with previous assignments corresponding respectively to the conversion of bulk and surface oxygen species [40]. Some similarities exist with H₂ consumption profiles obtained on binary V₂O₅/CeO₂ systems [41] with a high temperature reduction near 681 °C corresponding to the transformation of CeVO₄ to CeVO₃. This assignment is also consistent with the estimate of the H/V ratio ~2 and the linear increasing of the temperature at the maximum of the H₂-consumption profile vs. the crystallite size of CeVO₄ emphasizing a loss of oxygen mobility with a crystallite growth. Regarding the low temperature signal, as aforementioned one can rule the minor participation of the bulk reduction of CeO₂ to this signal which should occur above 708 °C [42] and is likely hidden by the prominent reduction of CeVO₄. On the other hand, this broad and weak contribution could reflect the reduction of surface Ce⁴⁺ species to Ce³⁺ both in CeO₂ and CeVO₄ with diffuse maxima appearing at 472 and 541 °C on the freshly-prepared sample (Fig. 5(a)). Those observations could also have different origins as suggested by Li et al. [43] from H₂-TPR experiments on VO_x-CeO₂ who also observed two weak contributions at low temperature at ~540 °C and ~580 °C [43]. These authors ascribed the former contribution to the reduction of surface VO_x species on smaller CeO₂ particles whereas the reduction of VO_x species on larger CeO₂ particles would occur at higher temperature. Such an interpretation would correctly explain the slight shift observed of this weak contribution becoming less intense on the aged sample at 600 °C and shifting to higher temperature due to the thermal sintering of CeO₂ as indicated in Table 1.

3.2. Surface characterization

3.2.1. XPS analysis

The chemical state of cerium, vanadium and oxygen and their relative surface concentrations were investigated by examining the characteristic Ce 3d, V 2p and O 1s core levels. Results are collected in Table 2. As exemplified, B.E. values for the V 2p_{3/2} core level close to 517.7 eV do not vary significantly and could be preferentially ascribed to V⁵⁺ [44]. More complex spectral features are usually observed on the Ce 3d photopeak (see Fig. S1 in Supplementary materials) with two distinct Ce 3d_{5/2} and Ce 3d_{3/2} signals which can be decomposed into different components (see Fig. S2 in Supplementary materials) characteristic of Ce³⁺ or Ce⁴⁺. The shape of the overall signal underlines a predominant formation of Ce³⁺ compared to Ce⁴⁺ [45]. Semi-quantitative analysis summarized in Table 2 confirms the prominent stabilization of Ce³⁺ through the estimation of the Ce⁴⁺/Ce³⁺ ratio in agreement with the formation of CeVO₄. Important information can be obtained from the comparison of the Ce⁴⁺/Ce³⁺ ratios underlining higher values on aged samples. Such a trend can be compared with spectral features of the O 1s photopeak characterized by two contributions on CeVO₄ at 530.5 eV and 532.0 eV reflecting the distribution at the surface of lattice oxygen O²⁻ (O^β) and adsorbed oxygen species (O^α) i.e. O₂⁻, O⁻ or OH groups [46,47]. O^α species are more active being more prone to create surface oxygen vacancies and defect sites which could have some consequences on the catalytic properties. A relatively good agreement between an increase in Ce⁴⁺/Ce³⁺ parallel to a decrease in O^α/O^β values underlines lower concentrations of surface oxygen vacancies. As a matter of fact, such a tendency can be correctly explained by a higher sensitivity of CeVO₄ to particle growth than CeO₂ with a rise in aging temperature as earlier discussed from the evolution of crystallite sizes in Table 1. Based on this statement, a gradual decrease of the surface vanadium species

Table 2Surface properties of CeVO₄ catalysts freshly-prepared from hydrothermal synthesis and after aging from XPS analysis and pyridine adsorption.

Catalyst	B.E. (eV) ^a		Surf. Composition ^a			Pyridine uptake ^b (μmol g ⁻¹)	
	Ce 3d _{5/2}	V2p _{3/2}	V/Ce	Ce ⁴⁺ /Ce ³⁺	O ^α /O ^β	100 °C	150 °C
Fresh	883.7	517.6	0.78	0.12	0.34	92.6	40.2
After SCR reaction ^c	n.m.	n.m.	n.m.	n.m.	n.m.	62.7	29.9
Aged at 500 °C	883.3	517.6	1.03	0.22	0.27	25.4	11.7
Aged at 600 °C	883.5	517.7	0.94	0.23	0.27	10.0	4.1

^a Binding energy values and surface composition from XPS analysis.^b From infrared spectroscopic measurements (see Fig. 6).^c After exposure to successive TPR reaction experiments with different molar NO/NO_x ratios.

should be similarly expected. In fact, the estimates of the surface atomic V/Ce ratio in Table 2 contradict this prediction revealing an increase in vanadium surface concentration on aged samples especially after aging at 500 °C. Such an observation underlines different competitive bulk and surface processes taking place during aging. Hence, parallel to thermal sintering, a partial extraction of vanadium species from the CeVO₄ lattice could be responsible of such surface vanadium enrichment on aged samples.

3.2.2. Surface acidity from pyridine adsorption-desorption experiments

Pyridine was adsorbed at 25 °C up to saturation coverage on degassed samples after evacuation under vacuum (10⁻³ mbar) at 450 °C. IR bands ascribed to the ring deformation of pyridine appear in the range 1400–1700 cm⁻¹ and allow the discrimination of Brønsted and Lewis sites on pre-adsorbed CeVO₄. Quasi-complete desorption of adsorbed pyridine was usually observed at 200 °C on fresh (see Fig. S3) and aged samples characterizing the presence of weak acid sites. Infrared bands at 1598 cm⁻¹ (ν_{8a}), 1574 (ν_{8b}), 1490 (ν_{19a}), 1441 cm⁻¹ (ν_{19b}) were previously ascribed to the vibrational modes of pyridine adsorbed on Lewis acid sites whereas IR bands located at 1640 cm⁻¹ (ν_{8a}), 1540 (ν_{19b}), are currently ascribed to pyridinium ion coordinated to Brønsted acid sites [48,49]. Let us note that Brønsted acid sites were not detected on fresh CeVO₄.

IR spectra recorded after evacuation at 100 °C and 150 °C are collected in Fig. 6 revealing the same tendencies with predominant Lewis acid sites. However, some peculiarities are clearly discernible on CeVO₄ aged at 500 °C (Fig. 6(A)-(a)) highlighting a slight strengthening of the pyridine adsorption on Lewis acid sites and the evidence of different type of Lewis acid sites. The most prominent observation is likely related to the appearance of two additional IR bands at 1639 and 1538 cm⁻¹ which characterize the presence of Brønsted acid sites. Normalized pyridine uptake have been estimated from the integration of IR bands by using the absorption coefficient of Lewis and Brønsted acid sites as reported elsewhere [28].

3.3. Selective catalytic reduction of NO_x by ammonia on CeVO₄

3.3.1. Preliminary observations from temperature-programmed-reaction experiments in fast and standard-SCR conditions

Concentration profiles for ammonia, NO_x and N₂ vs. temperature measured in standard- and fast SCR conditions on aged CeVO₄ samples at 500 °C and 600 °C are reported respectively in Figs. 7 and 8. The nitrogen mass balance was systematically verified with no significant variation below 2%. As observed in both figures, the conversions recorded in fast-SCR conditions are much higher compared to standard conditions especially at low temperature. As earlier explained, a faster re-oxidation of vanadate species by NO₂ and/or adsorbed nitrates rather than oxygen could satisfactorily explain these results [17,18]. CeVO₄ aged at 500 °C is characterized by an exceptional selectivity with a complete NO_x

conversion to nitrogen compared to a wide variety of mixed oxides especially above 350 °C when ammonia oxidation becomes predominant [14,24,50–52]. Let us note that similar catalytic features were also characterized on the fresh CeVO₄ samples. Traces of NO₂ were detected in standard NO conditions but not in significant amount. It is also noticeable that there is no significant divergence observed on the concentration profiles of NO and ammonia with a rise in temperature related to a significant ammonia oxidation to NO on CeVO₄ aged at 500 °C emphasizing a moderate competitive ammonia oxidation compared to previous observations on vanadia based-catalysts [14,21]. In the whole temperature range the molar N₂/NO and NO/NH₃ ratios close to 1 are characteristic of the standard-SCR conditions.

An ageing at 600 °C, slightly alter the catalytic performances in standard-SCR conditions above 250 °C with higher residual NO concentrations and lower concentrations of nitrogen formed compared those measured after aging at 500 °C. In fast-SCR conditions, a loss of NO reduction to nitrogen is also noticeable above 350 °C but N₂O does not form up to 450 °C. As illustrated, the concentration profiles for NO and NH₃ concentration diverge above 450 °C accompanied with lower nitrogen concentrations which evidence the occurrence of ammonia oxidation to NO. It is worthwhile to note that only traces of N₂O (below 20 ppm) were detected in fast-SCR conditions above 450 °C (see Fig. 8(a)). Fig. 9 compares the conversion curves for NO_x to nitrogen vs. temperature recorded on fresh and aged samples. In the particular case of fresh CeVO₄, an additional experiment was achieved considering the same NO/NO_x ratio of 1 investigated during the first cycle to verify if deactivation takes place in the course of the reaction. As observed in Fig. 9(b), no deactivation phenomena occurs, on the contrary a slight rate enhancement in NO conversion is noticeable. A typical volcano-type curve corresponding to a lowest conversion at the maximum (below 50%) characterizes the aged sample at 600 °C likely related to a preferential oxidation of ammonia to NO at high temperature. Surprisingly, aging at 500 °C does not induce a loss of conversion above 400 °C, the conversion becoming even better than that recorded on the fresh catalyst in this temperature conditions stabilizing near 80% in standard SCR-conditions. The same trends are also discernible in fast-SCR conditions, above 350 °C, demonstrating the superior catalytic properties of CeVO₄ aged at 500 °C in this temperature range (see Fig. 9(a)).

3.3.2. Kinetic behavior in standard-SCR conditions below 300 °C

Kinetics parameters have been tentatively estimated from temperature-programmed conversions measured below 300 °C in standard-SCR conditions (see Fig. 9(b)). As described in the experimental section, no significant external mass transfer limitations were characterized on fresh CeVO₄ in this range of temperature and conversion. Generally, the power-low rate expression given by Eq. (3) as a function of the concentration of the reactants and the rate constant k correctly models the ammonia SCR reaction.

$$r = k [NO]^\alpha [NH_3]^\beta [O_2]^\gamma \quad (3)$$

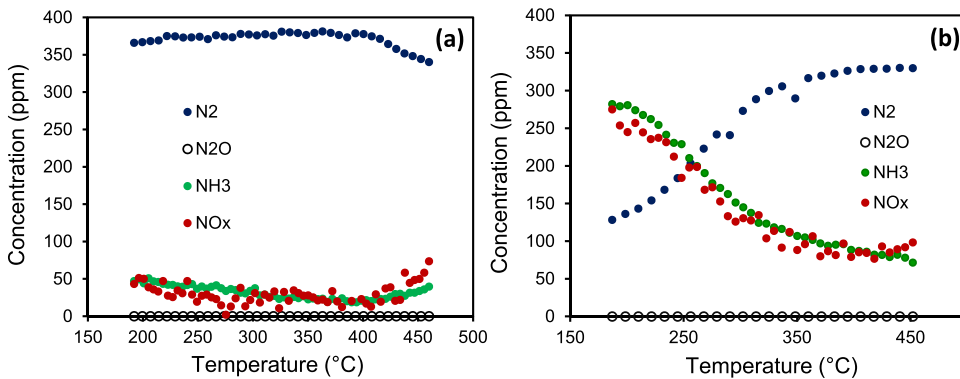


Fig. 7. Temperature-programmed concentration profiles vs. temperature recorded on CeVO₄ aged at 500 °C in fast-SCR conditions (a) and standard SCR conditions (b).

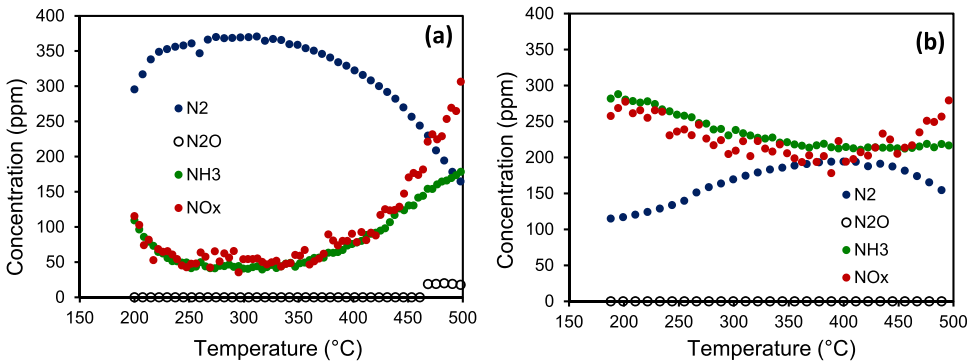


Fig. 8. Temperature-programmed concentration profiles vs. temperature recorded on CeVO₄ aged at 600 °C in fast-SCR conditions (a) and standard SCR conditions (b).

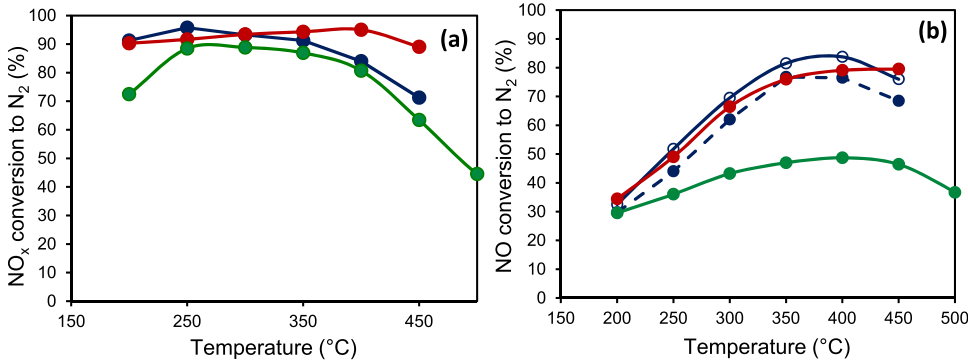


Fig. 9. Temperature-programmed NO conversion curves recorded during the ammonia-selective reduction of NO_x in fast- (a) and standard-SCR conditions (b) on fresh CeVO₄ (full symbol in blue); after SCR reaction (open symbol in blue); after aging at 500 °C (full symbol in red); after aging at 600 °C (full symbol in green). (For interpretation of the references to colour in this figure legend, the reader is referred to the web version of this article.)

α , β and γ are the reaction orders with respect to the concentration of NO, NH₃ and O₂ respectively. Earlier investigations over a wide variety of catalysts [3,20,53,54] found that $\alpha \sim 1$ and $\beta \sim 0$ below 300 °C. This is consistent with the fact that ammonia strongly chemisorbed whereas NO is hardly adsorbed on vanadia surface [3]. In a large excess of oxygen, a first-order kinetic equation can be assumed according to Eq. (4).

$$r = A \exp \left(-\frac{E_a}{RT} \right) [NO] \quad (4)$$

The first order rate constant k can be calculated at different temperature by using Eq. (5) valid for an integral reactor regime, W and F_0 being respectively the weight of catalyst and the total flow rate.

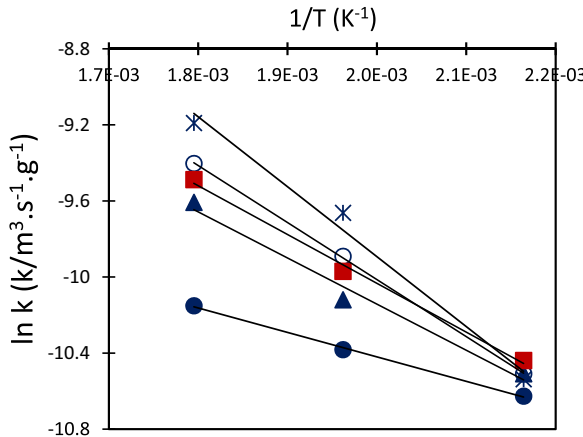
$$k = \frac{F_0}{W} \ln \left(\frac{1}{1 - X_{NO_x}} \right) (L \cdot g^{-1} \cdot s^{-1}) \quad (5)$$

Afterwards, the pre-exponential and apparent activation energy values can be estimated from the intercepts and the slopes of the Arrhenius plots in Fig. 10. As observed in Table 3, the apparent activation values (E_{app}) are rather low approximately roughly equal to half the current values reported in the literature varying in the range 35–55 kJ mol⁻¹ [3,53,55]. Such an observation could reflect: (i) some limitations due to internal mass transfer phenomena with observed activation energy $E_{obs} \sim E_a/2$ –(ii) the complexity of surface processes due the coexistence and the cooperation of CeO₂ and CeVO₄ with a rise in temperature in the overall standard-SCR process. The evaluation of internal mass transfer limitation was achieved through the estimation of the Weisz-Prater criterion.

For a first-order reaction the Weisz-Prater criterion is given by Eq. (6) with r_{obs} the observed reaction rate expressed in mol m³ s⁻¹, C_{obs} is the observed concentration solution in mol.m⁻³, $D_{eff,NO}$ the effective diffusivity for NO expressed in m² s⁻¹ in the range

Table 3Kinetic parameters recorded on fresh and aged CeVO₄.

Catalyst	E _{app} (kJ mol ⁻¹)	Pre-exponential factor, A (m ³ s ⁻¹ g ⁻¹)	k ^{a,b} (m ³ s ⁻¹ g ⁻¹)	Normalized k ^b (μmol s ⁻¹ m ⁻²)	TOF ^b (s ⁻¹)
Fresh	20.1 ± 2.0	(4.4 ± 0.5) × 10 ⁻³	2.7 × 10 ⁻⁵	24.0	28
After SCR reaction	24.9 ± 2.5	(15.5 ± 1.6) × 10 ⁻³	2.7 × 10 ⁻⁵	30.7	37
Aged at 500 °C	21.3 ± 2.5	(6.5 ± 0.7) × 10 ⁻³	2.9 × 10 ⁻⁵	70.6	101
Aged at 600 °C	10.7 ± 1.1	(0.4 ± 0.1) × 10 ⁻³	2.4 × 10 ⁻⁵	171.5	243
Aged at 600 °C + CeO ₂	30.5 ± 3.1	(65.5 ± 6.6) × 10 ⁻³	2.4 × 10 ⁻⁵	n.m	n.m

^a Calculated from Eq. (5).^b T(reaction) = 200 °C.**Fig. 10.** Arrhenius plots recorded during standard NH₃-SCR reaction on Fresh CeVO₄ (▲) on used CeVO₄ after reaction (○), on aged CeVO₄ at 500 °C (■) an CeVO₄ aged at (600 °C) (●) on a physical mixture CeVO₄ aged at 600 °C + CeO₂ (*).

1.0–1.5 × 10⁻⁶ m s⁻¹ [56] and L = d_p/6 the volume to surface ratio of the grain in m. Our calculations led to values lower than 0.4 for the Weisz-Prater criterion which fulfill the boundary conditions given by Eq. (6) emphasizing the fact that internal diffusion limitations should not occur significantly [57].

$$\frac{r_{obs} L^2}{C_{obs} D_{eff,NO}} < 1 \quad (6)$$

The abnormally low value of the apparent activation energy for the aged sample at 600 °C could reflect the occurrence of significant external diffusion phenomena. However, this low value could be also representative of complex chemical processes induced by structural surface changes during aging associated to particle sintering of CeO₂ and CeVO₄, partial extraction and segregation of more reducible V⁵⁺ species at the surface as observed from XRD, NMR, H₂-TPR and XPS analysis. In order to evaluate the role of ceria coexisting in minor concentration in CeVO₄, an extra experiment was performed on a physical mixture composed of the aged CeVO₄ sample at 600 °C with 10 wt.% CeO₂ aged in the same experimental conditions. As exemplified in Fig. S4, a higher conversion is observable on the physical mixture which underlines the redox properties of ceria and its capacity to oxidize more readily NO to NO₂ at low temperature leading to a gain in SCR conversion. Such a rate enhancement is also accompanied with a sharp increase of the apparent activation energy shifting from 10.7 on aged CeVO₄ at 600 °C to 30 kJ mol⁻¹ on the physical mixture. Such observations could highlight changes in the slow step governing the standard-SCR due to the participation of CeO₂ on fresh and aged sample at 500 °C whereas its contribution would be minimized on aged sample at 600 °C because of significant sintering of CeO₂ (see Table 1).

Normalized rate constants were estimated at 200 °C expressed per m² and TOF values have been also tentatively calculated in standard-SCR conditions on the basis of the dosage of Lewis acid sites from pyridine uptakes (see Table 2). This method of calcula-

tion differs from that currently used for supported vanadium based catalysts assuming a vanadium dispersion of 100% corresponding to the formation of isolated vanadate species [8,9] or from oxygen titration by chemisorption [58]. Similar trends on TOF and normalized rate values in Table 3 are noticeable increasing in the same proportion as a function the aging temperature. The highest value obtained on CeVO₄ aged at 600 °C seems consistent with the explanation given by Khodakov et al. [58] in case of the formation of polyvanadate species intrinsically more active in the oxidative dehydrogenation reactions than monovanadate formed at low coverages and would also match the lowest selectivity observed due to the involvement of ammonia oxidation also enhanced when monovanadates species aggregate into polymeric species.

4. Discussion

4.1. Tentative establishment of structure-activity relationship on CeVO₄: influence of aging

This study reports the behavior of bulk CeVO₄ catalysts for the selective reduction of NO_x by ammonia. They were prepared by hydrothermal synthesis and aged at 500 °C and 600 °C in air containing 10 vol.% H₂O. The zircon-type structure of CeVO₄ is obtained after hydrothermal synthesis without additional calcination step and preserved after aging. An important parameter is related to the coexistence of low amount of CeO₂ with CeVO₄. Subsequent thermal aging treatment in wet atmosphere shows that CeVO₄ is more sensitive to crystallite growth than CeO₂. In fact, the thermal sintering of CeO₂ is only detectable at 600 °C. It is worthwhile to note that no V₂O₅ was detected and no loss of vanadium due to sublimation was characterized on aged samples from elemental analysis.

As mentioned in the introduction, trying to relate surface properties to the kinetic behavior is relatively uneasy for supported and especially unsupported vanadium based catalysts combining redox and acidic functionalities basically associated with V⁵⁺-OH as acid sites for ammonia adsorption and redox V⁵⁺-O sites, for activating adsorbed ammonia species. According to this explanation, the stabilization of Ce³⁺ and V⁵⁺ inside the zircon-type structure of CeVO₄ could *a priori* deteriorate the catalytic properties. In fact, the comparison in Table 4 clearly reveals the superiority of CeVO₄ compared to supported vanadia based systems with a rate enhancement observed after aging.

Important information are provided by surface physicochemical analysis to explain this peculiar catalytic behaviour. XPS analysis shows an increase of the surface vanadium composition on aged samples with the highest atomic V/Ce ratio after aging at 500 °C. IR spectroscopic measurements showed predominantly the presence of Lewis acid sites. However, additional IR bands on the aged sample at 500 °C appearing at 1538 and 1639 cm⁻¹ from pyridine adsorption characterize Brønsted acid sites which could be tentatively related a predominant formation of V=O²⁺ species associated to different hydration degree and in the density of OH groups coordinated to the vanadium ions. These observations seem in rel-

Table 4

Comparison of the SCR performance of various supported and bulk vanadium-based catalysts.

Catalyst	Feed gas composition	T(reaction) (°C)	X _{NO}	Normalized k ^a (μmol s ⁻¹ m ⁻²)	N ₂ Selectivity	Ref.
V ₂ O ₅ -WO ₃ /TiO ₂ 55 m ² /g	500 ppm NO, 500 ppm NH ₃ , 3 vol.% O ₂ 10 vol.% H ₂ O – W/Q ₀ = 2.7 × 10 ⁻² g.h.L ⁻¹	200	0.95	23	85 at 400 °C	[24]
V ₂ O ₅ (1.5)-MoO ₃ (6) /TiO ₂ - 68 m ² /g	1000 ppm NO, 1000 ppm NH ₃ W/Q ₀ = 2.2 × 10 ⁻² g.Lh ⁻¹	200	0.30	2.7	48% at T = 427 °C	[62]
VO _x /CeO ₂ (V/Ce = 7.5) 110 m ² /g	500 ppm NO, 500 ppm NH ₃ , 3 vol.% O ₂ W/Q ₀ = 0.8 × 10 ⁻² g.h.L ⁻¹	200	0.60	11.9	95.3% at 400 °C	[59]
V ₂ O ₅ -WO ₃ /TiO ₂ Calc. 500 °C (63 m ² /g) Calc. 800 °C (17 m ² /g)	750 ppm NO, 840 ppm NH ₃ , 2 vol.% O ₂ W/Q ₀ = 2.2 × 10 ⁻² g h L ⁻¹	200	0.18 ^b	2.6	82.5% at 500 °C	[39]
CeVO ₄ 32 m ² /g	500 ppm NH ₃ , 500 ppm NO _x , 5 vol.% O ₂ W/Q ₀ = 3 × 10 ⁻² g h L ⁻¹	200	0.58	10.3	73.5% at 400 °C	[60]
Fresh CeVO ₄ 46.6 m ² /g	400 ppm NH ₃ , 400 ppm NO _x , 8 vol.% O ₂ , 10 vol.% CO ₂ , 10% H ₂ O W/Q ₀ = 4 × 10 ⁻³ g h L ⁻¹	200	0.32	24.0	100% N ₂ [175–500 °C]	This study
Aged CeVO ₄ at 600 °C 5.8 m ² /g	400 ppm NH ₃ , 400 ppm NO _x , 8 vol.% O ₂ , 10 vol.% CO ₂ , 10% H ₂ O W/Q ₀ = 4 × 10 ⁻³ g h L ⁻¹	200	0.30	171.5	100% N ₂ [175–460 °C]	This study

^a Calculated according to the mass balance Eq. (5) for an integral reaction assuming a first order kinetic. Normalized rate constants expressed per m² were calculated by taking the specific surface area into account.

^b In the presence of 10 vol.% H₂O and 100 ppm SO₂–.

^c In the presence of 5 vol.% H₂O.

ative good agreement with spectral features from ⁵¹V NMR and EPR measurements. The structural distortion on the zircon-type structure suggested from the shift observed on ⁵¹V NMR spectra can be compared to the detection of paramagnetic V(+IV) species from EPR spectroscopies and would suggest the formation of more reducible vanadium species than isolated V⁵⁺ in tetrahedral environment of the zircon-type structure of CeVO₄. The formation of more reducible VO_x species at the surface is also consistent with H₂-TPR observations especially on CeVO₄ aged at 500 °C. In this sense the significant increase in the V/Ce observed from XPS on this latter sample jointly with the formation on Brønsted acid sites could be explained by a partial extraction of vanadate and their segregation at the surface of CeVO₄ during aging into well-dispersed monomeric VO_x species. At increasing aging temperature the slight lessening of the surface V/Ce ratio (see Table 3) as well as the disappearance of Brønsted acid sites on the aged sample at 600 °C (Fig. 6A(d) and B(d)) could reflect a more extensive extraction and aggregation processes of surface monomeric vanadate species to polymeric species such as O=V—O—V=O [59] in agreement with previous observations reported by Nova et al. on V₂O₅-WO₃/TiO₂ who also observed an agglomeration of monomeric to more reducible polymeric at increasing calcination temperature.

To go a little farther to the discussion we have compared the TOF values calculated at 200 °C in Table 3 to the surface V/Ce ratio. As illustrated in Fig. 11 a maximum is observed corresponding to the surface composition of CeVO₄ aged at 600 °C. Similar observations reproduce for TOF measured at 250 °C. The lowest TOF value obtained on the fresh sample are consistent with earlier interpretations provided by Huang et al. [60] who suggested moderate valence changes between Ce⁴⁺ and Ce³⁺ stabilized inside the CeVO₄ lattice further blocking the redox behavior of vanadium. This conclusion is also in relative agreement with usual observations showing that the SCR usually proceeds more slowly on unreduceable metal oxide sites i.e. typically on fresh CeVO₄.

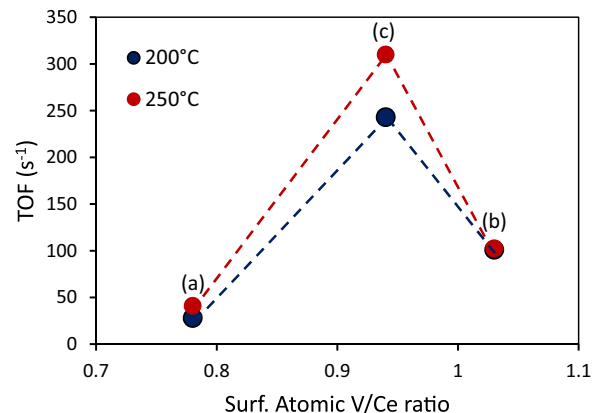


Fig. 11. Surface V concentration dependency of the Turn-Over-Frequency calculated on fresh (a) and aged CeVO₄ samples at 500 °C (b) and 600 °C (c) during the standard ammonia-SCR reaction.

The experiment of the physical mixture containing aged CeO₂ and CeVO₄ at 600 °C underlines the crucial role played by Ce⁴⁺/Ce³⁺ of CeO₂ instead of CeVO₄ with a sharp enhancement in the rate of NO_x reduction to nitrogen as seen in Fig. S4. Basically, such rate enhancement could be related to an increasing density of sites provided by CeO₂ for oxidizing more readily NO to NO₂ and then insuring a faster re-oxidation of V(+IV) to V(+V) compared to O₂ in standard conditions. This observation would also suggest at least on fresh and aged CeVO₄ at 500 °C that redox sites at the vicinity of acid sites could not be formally a prerequisite if we consider separately CeO₂ and CeVO₄ as unique active phases.

Returning to CeVO₄ aged at 600 °C, lower concentration of Ce⁴⁺/Ce³⁺ is expected because CeO₂ becomes more sensitive to thermal sintering at that temperature which means that this should be related to a loss of catalytic properties. Based on this fact, the highest TOF calculated on aged CeVO₄ at 600 °C does not properly

match with this explanation but could be reasonably interpreted by a compensation effect due to the restoration of the redox behavior of V^{5+}/V^{4+} as a result of partial diffusion of vanadium species at the surface and subsequent agglomeration into polymeric species in agreement with previous information showing increasing TOF values associate with the polymerization of isolated VO_x species [9,58].

The strength of acid sites and their composition is still a matter of discussion especially the involvement of Lewis and Brønsted sites and surface vanadia species. Our IR spectroscopic observations essentially led to the observation of Lewis acid sites except for $CeVO_4$ aged at 500 °C with a minor contribution of Brønsted acid sites. Recently, Peng et al. [59] characterized the presence of $CeVO_4$ on VO_x/CeO_2 and attributed its formation to the creation of Brønsted sites whereas VO_x and CeO_2 would originate Lewis acid sites. As a matter of fact, our observations partly disagree with those previous assignments at least for the aged sample at 500 °C. Indeed, bulk $CeVO_4$ exhibits essentially Lewis acidic properties whereas the creation of Brønsted acid sites on aged samples would be more related to the segregation of VO_x species as exemplified on $CeVO_4$ aged at 500 °C. This formation could partly explain why this sample retains at high temperature the highest selective conversion of NO_x to nitrogen (see Fig. 9). On the other hand, subsequent aggregation on VO_x to form polyvanadate species would suppress Brønsted acidity and then restoring the participation of weakly acidic Lewis acid sites on the aged sample at 600 °C.

All these observations seem consistent with the involvement of a dual site mechanism on aged catalysts with the participation of V-O-V bridged at the vicinity of V-O-Ce site especially on $CeVO_4$ aged at 600 °C. Such a conclusion seems to be in relative good agreement with previous conclusions drawn by Wachs et al. [9] who concluded that a higher $DeNO_x$ activity could involve a pair of sites combining a redox site and a nearest-neighbor non reducible site. Taking this viewpoint into account and returning to the abnormally low value for the apparent activation energy, the difference observed with the values estimated on fresh and aged samples could reflect changes in the nature of the slow step with the occurrence of surface diffusion processes on the aged sample at 600 °C. Indeed, previous transient kinetic investigations also found very low values for activation energy values in the range 5–8 kJ mol^{−1} ascribed to spill-over effect on Pd/Al_2O_3 [61]. While the system investigated in this study is very different, such a hypothesis could be suggested in the particular case of a dual site mechanism. The weaker ammonia adsorption on $CeVO_4$ aged at 600 °C compared to the aged sample at 500 °C could support such an assumption in agreement with the explanation provided by Gao et al. [20] who suggested that ammonia weakly bonded to acid sites on Cu/SSZ-13 could diffuse more easily to redox Cu-ion sites. According to this assumption, the interface between surface VO_x species and $CeVO_4$ could play an important role for aged samples increasing at higher aging temperature.

4.2. Bulk vs. supported vanadia based catalysts: unprecedented catalytic properties of $CeVO_4$

Major information compared to conventional and modified supported vanadium based catalysts are summarized in Table 4 related to: (i) the absence of N_2O formation previously related to the preferential ammonia oxidation at high temperature and preferential decomposition of ammonium nitrates in fast conditions – (ii) a greater stabilization of dispersed vanadate species at the surface compared to supported catalysts preserving their selectivity behaviour – (iii) higher normalized rates on aged catalysts at low temperature which makes this solid suitable for further practical developments. Regarding, the estimates of normalized rate constants expressed per m² in Table 4, their comparison highlights the

importance of assessing the catalytic properties close to real operating conditions with the presence of gaseous water [21,24,39,62,63].

As exemplified freshly-prepared $CeVO_4$ samples are in most cases intrinsically more active than VO_x entities dispersed on various supports materials essentially TiO_2 [24,39] or CeO_2 [21]. Interestingly, such a trend accentuates on aged $CeVO_4$ sample at 600 °C with increasing normalized rate of one order of magnitude. Remarkably, a complete selectivity to nitrogen production is preserved in the whole range of temperature irrespective of the aging conditions. As a matter of fact, such a peculiar activity behavior was earlier observed on $V_2O_5-WO_3/TiO_2$ with a rate enhancement obtained in the SCR reaction on calcined catalysts at 800 °C instead of 500 °C in dry conditions [39]. On the contrary, the authors observed a detrimental effect on the selectivity to N_2 production due to the sintering of TiO_2 and subsequent aggregation of isolated vanadate to polymeric species suggested as intrinsically more active but unfortunately less selective. Obviously, we also observed a slight detrimental effect of the selectivity behavior on $CeVO_4$ aged at 600 °C likely but due to ammonia oxidation to NO which explains the volcano-type curve observed in Figs. 8 and 9 (a). Finally, the peculiar behavior of the aged sample at 500 °C at high temperature is remarkable as it retains the highest conversion level and a good selectivity which emphasize the fact that the competitive ammonia oxidation to NO would be likely less-favored compared to the fresh $CeVO_4$ catalyst.

5. Conclusion

The catalytic properties of bulk $CeVO_4$ catalysts prepared by hydrothermal synthesis have been investigated in the ammonia-selective catalytic reduction of NO_x . Particular attention was paid to the behavior of aged samples under wet atmosphere at 500 °C and 600 °C in standard- and fast-conditions revealing superior performances, based on the comparison of TOF, and higher stability than supported vanadia based catalysts with slow agglomeration processes avoiding the ultimate formation of less stable and selective V_2O_5 clusters. Isolated $V(+V)$ species remains essentially stabilized in tetrahedral coordination inside the zircon-type structure of $CeVO_4$. The coexistence of low concentration of Ce^{4+} stabilized as CeO_2 was found as a key parameter for freshly-prepared samples with cooperative effects on the rate of NO conversion to nitrogen regardless of the operating conditions. Hence, the lowest redox properties of weak reducible $CeVO_4$ mixed oxide can be counterbalanced by those characterizing CeO_2 insuring a faster NO oxidation to NO_2 . Aging leads to significant changes on the redox and acidic properties which can be reasonably compared to catalytic properties. The most important chemical process modifying the surface properties can be related to a slight segregation of VO_x species ascribed to partial extraction of unreduceable isolated V^{5+} species in octahedral environment. Such process is accelerated after aging at 600 °C but moderated since the ultimate formation of V_2O_5 oxide clusters was not characterized. On the other hand, such reconstructions modify significantly the acidic properties with the appearance of Brønsted acid sites on aged sample at 500 °C and the restoration of superior redox properties ascribed to V^{5+}/V^{4+} instead of Ce^{4+}/Ce^{3+} on fresh samples. Consistently, more polymerized VO_x species originate higher TOF values at low temperature but a slight detrimental effect on the selectivity was observed at high temperature due to the occurrence of the competitive ammonia oxidation to NO. All these observations could suggest a pair of sites combining a redox site and a nearest-neighbor non reducible site on aged sample ascribed respectively to V-O-V and V-O-Ce surface structures. An additional creation of Brønsted acid sites characterized on aged samples at 500 °C was not ascribed to $CeVO_4$ but more likely to well-dispersed monomeric $V=O^{2+}$ resulting to the extraction of

V^{5+} and a moderate agglomeration to subsequent more polymeric species taking place at more elevated aging temperature.

Acknowledgments

This work has achieved within a research project supported by the French National Agency for Research (UreeNOx Project, Ref. ANR-11-VPTT-002). We would like to thank Olivier Gardoll, Laurence Burylo, Jean-Charles Morin and Martine Trentesaux for their technical support for Thermal analysis, XRD, infrared spectroscopy and XPS measurements respectively.

Appendix A. Supplementary data

Supplementary data associated with this article can be found, in the online version, at <http://dx.doi.org/10.1016/j.apcatb.2017.06.049>.

References

- [1] P. Forzatti, L. Lietti, *Heterogeneous Chem. Rev.* 3 (1996) 33–51.
- [2] G. Busca, L. Lietti, G. Ramis, F. Berti, *Appl. Catal. B* 18 (1998) 1–36.
- [3] M. Inomata, A. Miyamoto, Y. Murakami, *J. Catal.* 62 (1980) 140–148.
- [4] J.A. Dumesic, N.-Y. Topsøe, H. Topsøe, Y. Chen, T. Slabiak, *J. Catal.* 163 (1996) 409–417.
- [5] N.-Y. Topsøe, *Science* 265 (5176) (1994) 1217–1219.
- [6] H. Kamata, K. Takahashi, C.U.I. Odenbrand, *J. Catal.* 185 (1999) 106–113.
- [7] C. Wang, S. Yang, H. Chang, Y. Peng, J. Li, *Chem. Eng. J.* 225 (2013) 520–527.
- [8] L. Lietti, G. Ramis, F. Berti, G. Toledo, D. Robba, G. Busca, P. Forzatti, *Catal. Today* 42 (1998) 101–116.
- [9] I.E. Wachs, G. Deo, B.M. Weckhuysen, A. Andreini, M.A. Vuurman, M. de Boer, M. Amiridis, *J. Catal.* 161 (1996) 211–221.
- [10] I. Giakoumelou, C. Fountzoula, C. Kordulis, S. Boghosian, *J. Catal.* 239 (2006) 1–12.
- [11] G. Ramis, G. Busca, V. Lorenzelli, P. Forzatti, *Appl. Catal.* 64 (1990) 259–278.
- [12] Z. Lian, F. Liu, H. He, *Ind. Eng. Chem. Res.* 53 (2014) 19506–19511.
- [13] R. Pérez Vélez, I. Ellmers, H. Huang, U. Bentrup, V. Schünemann, W. Grünert, A. Brückner, *J. Catal.* 316 (2014) 103–111.
- [14] G. Madia, M. Elsener, M. Koebel, F. Raimondi, A. Wokaun, *A. Appl. Catal. B* 39 (2002) 181–190.
- [15] [4] F. Can, X. Courtois, S. Berland, M. Seneque, S. Royer, D. Duprez, *Catal. Today* 257 (2015) 41–50.
- [16] J. Jansson, *Urea-SCR Technology for DeNO_x After Treatment of Diesel Exhausts*, in: I.E. Nova (Ed.), Tronconi, Springer Science and Business Media, New York, 2014, pp. 65–96.
- [17] I. Nova, C. Ciardelli, E. Tronconi, D. Chatterjee, B. Bandl-Konrad, *Catal. Today* 114 (2006) 3–12.
- [18] M. Koebel, G. Madia, F. Raimondi, A. Wokaun, *J. Catal.* 209 (2002) 159–165.
- [19] M. Casanova, J. Llorca, A. Sagar, K. Schermanz, A. Trovarelli, *Catal. Today* 241 (2015) 159–168.
- [20] F. Gao, N.M. Washton, Y. Wang, M. Kollár, J. Szanyi, C.H.F. Peden, *J. Catal.* 331 (2015) 25–38.
- [21] M. Yates, J.A. Martín, M.A. Martín-Luengo, S. Suárez, J. Blanco, *Catal. Today* 107–108 (2005) 120–125.
- [22] W. Shan, F. Liu, H. He, X. Shi, C. Zhang, *Catal. Today* 184 (2012) 160–165.
- [23] M.V. Martinez-Huerta, J.M. Coronado, M. Fernandez-Garcia, A. Iglesia-Juez, G. Deo, J.L.G. Fierro, M.A. Bañares, *J. Catal.* 225 (2004) 240–248.
- [24] L. Chen, J. Li, M. Ge, *J. Phys. Chem. C* 176 (2009) 21177–21184.
- [25] E.V. Tsipis, V.V. Kharton, N.P. Vyshatko, A.L. Shaula, J.R. Frade, *J. Sol. State Chem.* 176 (2003) 47–56.
- [26] B. Xie, G. Lu, Q. Dai, Y. Wang, Y. Guo, *J. Clust. Sci.* 22 (2011) 555–561.
- [27] S. Gillot, J.P. Dacquin, C. Dujardin, P. Granger, *Top. Catal.* 59 (2016) 987–995.
- [28] J. Goscianska, M. Ziolek, E. Gibson, M. Daturi, *Catal. Today* 152 (2010) 33–41.
- [29] L. Chen, *Mat. Lett.* 60 (2006) 1859–1862.
- [30] M.A. Bañares, I.E. Wachs, *J. Raman Spectrosc.* 33 (2002) 359–380.
- [31] S. Xie, E. Iglesia, A.T. Bell, *J. Phys. Chem. B* 105 (2001) 5144–5152.
- [32] B.M. Reddy, A. Khan, *Langmuir* 19 (2003) 3025–3030.
- [33] P.G.W.A. Kompio, A. Brückner, F. Hiper, G. Auer, E. Löffler, *J. Catal.* 286 (2012) 237–247.
- [34] J. Matta, D. Courcot, E. Abi-Aad, A. Aboukais, *Chem. Mater.* 14 (2002) 4118–4125.
- [35] R. Cousin, E. Abi-Aad, S. Capelle, D. Courcot, J.F. Lamonier, A. Aboukais, *J. Mater. Sci.* 42 (2007) 6188–6196.
- [36] P. Concepcion, H. Knözinger, J.M. Lopez Nieto, A. Martinez-Arias, *J. Phys. Chem. B* 106 (2002) 2574–2582.
- [37] G. Busca, G. Ramis, V. Lorenzelli, *J. Mol. Catal.* 50 (1989) 231–240.
- [38] A.M. Prakash, L. Kevan, *J. Phys. Chem. B* 104 (2000) 6860–6868.
- [39] I. Nova, L. dall'Acqua, L. Lietti, E. Giamello, P. Forzatti, *Appl. Catal. B* 35 (2001) 31–42.
- [40] Z. Wu, A.J. Rondinone, I.N. Ivanov, S.H. Overbury, *J. Phys. Chem. C* 115 (2011) 25368–25378.
- [41] H. Zhao, S. Bennici, J. Cai, J. Shen, A. Auroux, *J. Catal.* 274 (2010) 259–272.
- [42] M.V. Martinez-Huerta, G. Deo, J.L.G. Fierro, M.A. Bañares, *J. Phys. Chem. C* 111 (2007) 18708–18714.
- [43] Y. Li, Z. Wei, F. Gao, L. Kovarik, R.A.L. Baylon, C.H.F. Peden, Y. Wang, *ACS Catal.* 5 (2015) 3006–3012.
- [44] M. Demeter, M. Neumann, W. Reichelt, *Surf. Sci.* 454–456 (2000) 41–44.
- [45] M. Romeo, K. Bak, J. El Fallah, F. Lenormand, L. Hilaire, *Surf. Int. Anal.* 2 (1993) 508–512.
- [46] M. Kang, E.D. Park, J.M. Kim, J.E. Yie, *Appl. Catal. A* 327 (2007) 261–269.
- [47] X. Lu, C. Song, S. Jia, Z. Tong, X. Tang, Y. Teng, *Chem. Eng. J.* 260 (2015) 776–784.
- [48] F. Hatayama, T. Ohno, T. Maruoka, T. Ono, H. Miyata, *J. Chem. Soc. Faraday Trans.* 87 (1991) 2629–2633.
- [49] T. Barzetti, E. Sellì, D. Moscotti, L. Forni, *J. Chem. Soc. Faraday Trans.* 92 (1996) 1401–1407.
- [50] M. Casanova, K. Schermanz, J. Llorca, A. Trovarelli, *Catal. Today* 184 (2012) 227–236.
- [51] M.A. Centeno, P. Malet, I. Carrizosa, J.A. Odriozola, *J. Phys. Chem. B* 104 (2000) 3310–3319.
- [52] M. Casanova, J. Llorca, A. Sagar, K. Schermanz, A. Trovarelli, *Catal. Today* 241 (2015) 159–168.
- [53] G. Qi, R.T. Yang, *J. Catal.* 217 (2003) 434–441.
- [54] Z. Ma, X. Wu, H. Härelind, B. Wang, *J. Mol. Catal. A* 423 (2016) 172–180.
- [55] X. Hu, M. Yang, D. Fan, G. Qi, J. Wang, J. Wang, T. Yu, W. Li, M. Shen, *J. Catal.* 341 (2016) 55–61.
- [56] N. Usberti, M. Jablonska, M. Di Blasi, P. Forzatti, L. Lietti, A. Beretta, *Appl. Catal. B* 179 (2015) 185–195.
- [57] K.B. Bischoff, *Chem. Eng. Sci.* 22 (1967) 525–530.
- [58] A. Khodakov, B. Olthof, A.T. Bell, E. Iglesia, *J. Catal.* 181 (1999) 205–216.
- [59] Y. Peng, C. Wang, J. Li, *Appl. Catal. B* 144 (2014) 538–546.
- [60] H. Huang, Y. Gu, J. Zhao, W. Wang, *J. Catal.* 326 (2015) 54–68.
- [61] Y. Renème, F. Dhainaut, S. Pietrzky, M. Chaar, A.C. van Veen, P. Granger, *Appl. Catal. B* 126 (2012) 239–248.
- [62] L. Casagrande, L. Lietti, I. Nova, P. Forzatti, A. Baikers, *Appl. Catal. B* 22 (1999) 63–77.
- [63] X. Zhao, L. Huang, H. Hu, X. Hu, L. Shi, *Appl. Catal. B* 183 (2016) 269–281.